The ShakeOut Scenario

Supplemental Study

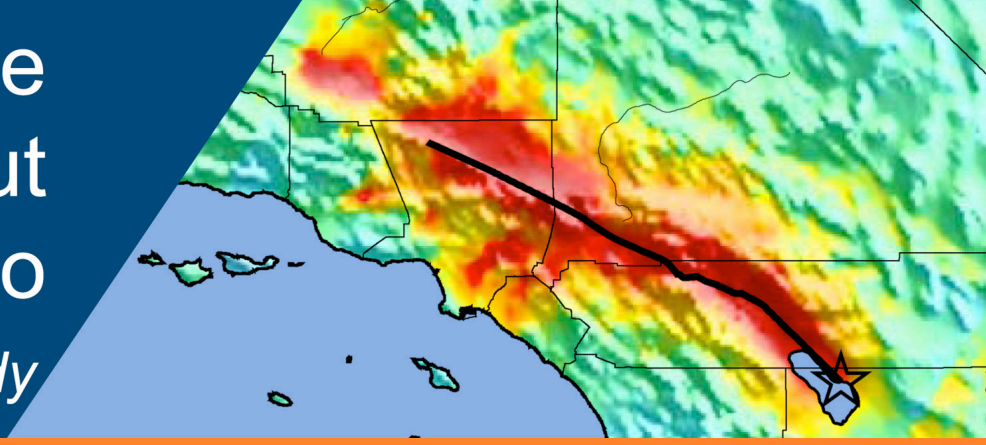

High-Rise Steel Buildings

Prepared for

United States Geological Survey

Pasadena CA

and

California Geological Survey

Sacramento CA

By

Swaminathan Krishnan and Matthew Muto

California Institute of Technology

Pasadena CA

May 2008

The ShakeOut Scenario:

U.S. Geological Survey Open File Report 2008-1150

California Geological Survey Preliminary Report 25 version 1.0

U.S. Geological Survey Circular 1324

California Geological Survey Special Report 207 version 1.0

Note: over the course of the ShakeOut Scenario, the project name evolved. Where a study mentions *the SoSAFE Scenario* or *San Andreas Fault Scenario,* it refers to what is now named the ShakeOut Scenario.

SHAKEOUT 2008: Tall Steel Moment Frame Building Response

Swaminathan Krishnan and Matthew Muto
California Institute of Technology

INTRODUCTION

In order to prepare for the next big earthquake on the San Andreas fault, the US Geological Survey (USGS) has started a year-long "DARE TO PREPARE" campaign that will culminate in the Great Southern California Shakeout Scenario in 2008. The scenario earthquake chosen is a magnitude 7.8 earthquake on the San Andreas fault with rupture initiating at Bombay Beach and propagating northwest a distance of roughly 304 km, terminating at Lake Hughes near Palmdale. In support of this shakeout exercise, Hudnut et al. (2007) have created a detailed, realistic earthquake scenario of an M_w 7.8 event on the southern San Andreas fault based on a wide variety of observations and constraints. The scenario earthquake initiates at Bombay Beach, breaks through the San Gorgonio Pass, and terminates at Lake Hughes (near Palmdale), sections of the San Andreas fault that last broke in 1680, 1812, and 1857. Through community participation in two Southern San Andreas Fault Evaluation (SoSAFE) workshops organized by the Southern California Earthquake Center (SCEC), a source model specific to the southern San Andreas fault has been constructed with constraints from geologic, geodetic, paleoseismic, and seismological observations (Figure 1).

Using this source model, Rob Graves of URS Corporation has simulated 3-component seismic waveforms on a uniform grid covering southern California. We have chosen 784 of these sites (shown using solid red triangles in Figure 2) to place 3-D computer models of three steel moment frame buildings in the 20-story class, and analyze these models subject to the simulated 3-component ground motion. The SCEC Community Velocity Model (Magistrale et al. 1996; Magistrale et al. 2000; Kohler et al. 2003), which allows for the modeling of the basin response down to a shortest period of approximately 2 s, was used for the ground motion simulations. While the top soil layer, also known as the geotechnical layer, is not included, a correction based on the shear wave speed at 30 m depth, V_s^{30}, is applied to the waveforms. The peaks of the three components of the lowpass-filtered and V_s^{30}-corrected velocity and displacement waveforms are shown in Figure 3. Peak velocities are in the range of 0-100 cm/s in the San Fernando valley, and 60-180 cm/s in the Los Angeles basin. Corresponding peak displacement ranges are 0-100 cm and 50-150 cm. This is in contrast to the peak displacements and velocities from the simulation of an 1857-like magnitude 7.9 earthquake on the San Andreas fault, with rupture initiating in Parkfield in central California and propagating a distance of about 290 km in a south-easterly direction (Krishnan et al. 2005, 2006a, 2006b). That simulation, performed using the SPECFEM3D code using the Harvard-LA Community Velocity Model (CVM) (Suss and Shaw 2003), also known as the SCEC CVM-H, resulted in peak velocities of the order of 1 m.s^{-1} in the Los Angeles basin, including downtown Los Angeles, and 2 m.s^{-1} in the San Fernando valley, and peak displacements of the order of 1 m and 2 m in the Los Angeles basin and San Fernando valley, respectively.

For the shakeout drill, USGS has commissioned us to provide a realistic picture of the impact of such an earthquake on the tall steel buildings in southern California. This is a very difficult task for various reasons. Firstly, no two buildings are alike and short of analyzing each existing building under the simulated ground motion, it is quite hard to paint a broad picture. Even if we are ready to perform these large number of analyses, the structural drawings of existing buildings are not easily available due to liability concerns. Secondly, there are quite a few limitations to both ground motion and structural simulations as elucidated in Krishnan et al. (2005, 2006a, 2006b). Having said this, the intent of the exercise is to get prepared for a big event, and it is not as important to be absolutely correct as it is to be in the ball-park so we know what we can expect from such an event, and are not caught flat-footed as in the case of hurricane Katrina. With this

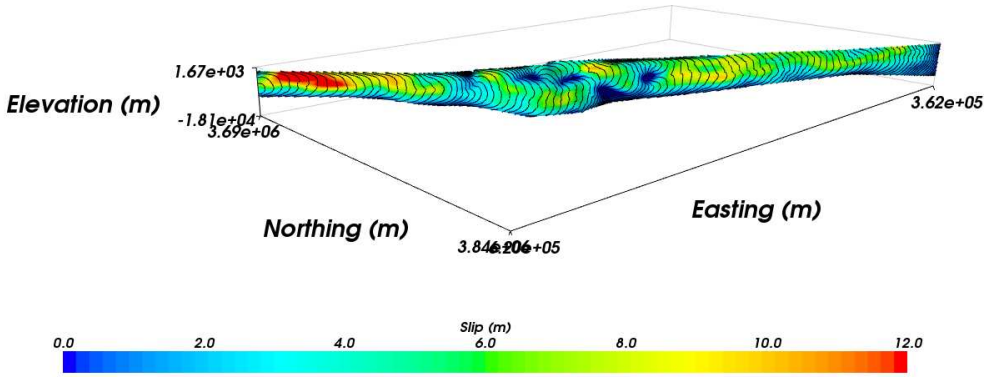

[A]

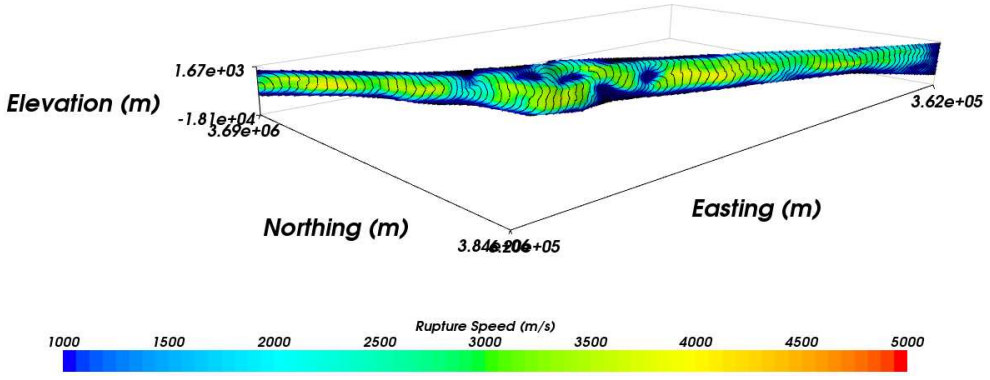

[B]

Figure 1: [A] Slip distribution used in the San Andreas fault shakeout scenario earthquake simulation. Peak slip at depth is about 12 m. The slip grows slowly and peaks towards the north-west before terminating abruptly. [B] Assumed rupture speed distribution. Super-shear rupture occurs in some portions of the fault.

in mind, we analyze three steel moment frame buildings in the 20-story class, orienting them in two different directions, considering perfect and imperfect realizations of beam-to-column connection behavior, subjecting them to the simulated 3-component ground motions at each of the 784 sites shown in Figure 2. We average the response from these 12 cases (3 buildings x 2 orientations x 2 connection susceptibility realizations), and combine this with the observed response of tall steel buildings in past earthquakes (unfortunately, there is not much data in this context) to provide a qualitative picture of one plausible outcome in the event of the big one striking southern California.

PERFORMANCE OF TALL STEEL BUILDINGS IN PAST EARTHQUAKES

Major steel building damage has only been observed in three earthquakes, the 1985 Mexico City earthquake, the 1994 Northridge earthquake, and the 1995 Kobe earthquake, although isolated cases of steel building damage has been observed in other instances. These observations, described in some detail in the next few sections, provide us pointers to the wide spectrum of possibilities in as far as damage to southern Californian steel buildings in a large San Andreas fault earthquake

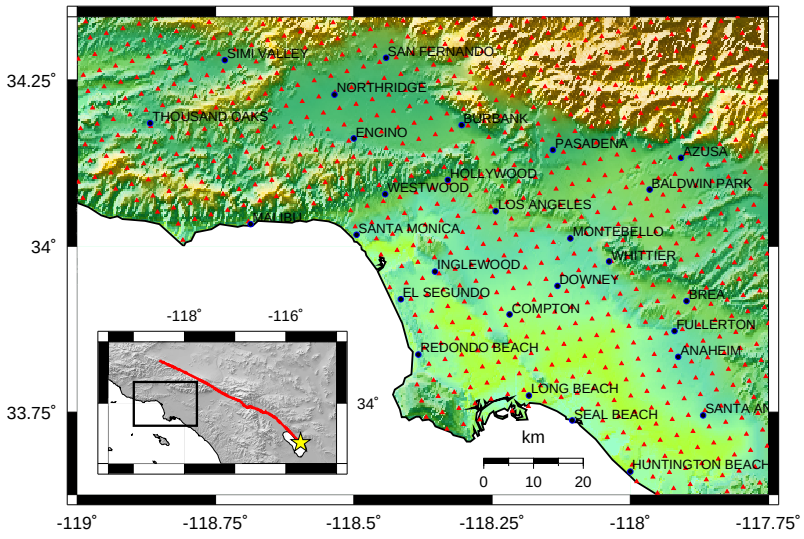

Figure 2: Geographical scope of the magnitude 7.8 San Andreas fault shakeout scenario earthquake simulation (the color scheme reflects topography, with green denoting low elevation and yellow denoting mountains): The solid red triangles represent the 784 sites at which seismograms are computed and buildings are analyzed. The red line in the inset is the surface trace of the hypothetical 304 km rupture of the San Andreas fault. The area enclosed by the blue polygon denotes the region covered by the 784 sites.

is concerned.

January 17, 1994, Magnitude 6.7 Northridge Earthquake, USA

The 1994 Northridge earthquake occurred on a previously unknown blind-thrust fault. Fortunately, rupture updip and towards the North resulted in significant directivity away from the heavily populated Los Angeles metropolitan region sending the greatest amount of energy into the mountains north of San Fernando valley (Wald et al. 1996). Yet, this earthquake revealed serious weaknesses in welded steel moment frame buildings in the greater Los Angeles region. Welded steel moment-frames were previously considered to be the most ductile of all the structural systems recommended by the building codes for seismic resistance. Ductile structural systems are capable of withstanding large inelastic deformations without significant degradation in strength, and remain stable without collapsing under strong ground motion. Following the Northridge earthquake, a number of steel moment frame buildings were found to have experienced brittle fractures in welded beam-to-column connections. Such nonductile behavior occurred in buildings with one to 26 stories (FEMA 2000d), with some of them as old as 30 years while others being erected at the time of the earthquake. The buildings were distributed throughout the region with some sites experiencing only moderate levels of ground shaking. Typically, fractures initiated at the root of the full penetration weld connecting the beam bottom flange to the column flange. Once initiated, the fractures progressed along a number of different paths, some progressing completely through the thickness of the weld, some developing into a crack in the column flange with the column flange separating from the rest of the column, some progressing further into the column web and across the panel zone, and finally in some instances the fractures cracked the

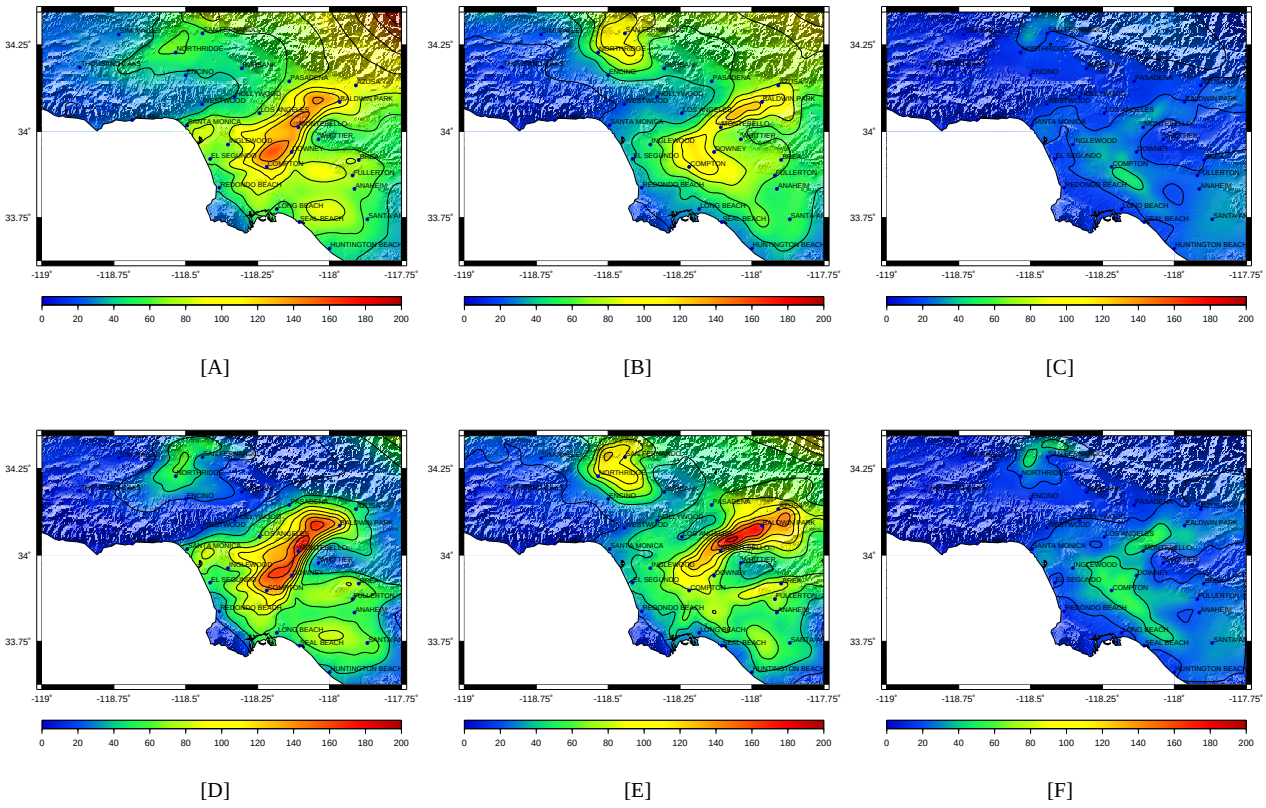

Figure 3: San Andreas fault shakeout scenario earthquake simulation: Peak ground motion under a S-to-N rupture (east [A], north [B], and vertical [C] components of displacement in "cm", and the corresponding components of velocity ([D], [E], and [F], respectively, in "cm/s".)

entire column cross-section (Figure 4). Such fractures can lead to a significant loss of stiffness and strength in the moment frames and can dramatically lower the capacity of the structure to resist collapse.

September 19, 1985, Magnitude 7.8 Mexico City Earthquake, Mexico

Steel construction is not common in Mexico City. Surprisingly, of the few steel buildings existent there at the time of the earthquake, two towers in a complex of five steel-frame buildings at Conjunto Pino Suarez apartment complex collapsed (Figures 5 and 6), and a third 21-story tower although remaining standing was leaning six feet out of plumb at the roof level (Figure 6[B]). Of the two buildings that collapsed, one was a 21-story structure and the other a 14-story structure. The 21-story structure collapsed onto the 14-story structure resulting in its collapse. These collapses have been attributed to the strong amplification of the lake bed on which parts of the city are located and the long-period nature of the ground motion (Beck and Hall 1986). The amplification was enabled by the long duration of the main shock resulting in a resonant buildup of seismic waves within the thick clay layer just beneath the surface. The three identical 21-story structures consisted of five 6m-bays in the long direction and two 6m-bays in the short direction. The lateral force-resisting system consisted of moment frames at all column lines with two bays in the short direction braced using X braces, and one bay in the long direction braced using V braces (Osteraas and Krawinkler 1990). These buildings were not pure moment-frame systems and the collapse is deemed to have occurred due to weld failure in the built-up box column and subsequent local buckling of the flanges (see Figure 5[B]). Nevertheless, the observed connection susceptibility to fracture in the Northridge earthquake,

in conjunction with motions such as those observed in Mexico City, could result in the kinds of collapses seen in Mexico City. In addition to demonstrating that even steel highrise structures can collapse, this earthquake brought to the fore the possibility of upper-story collapses in midrise and highrise structures, due in part to the pounding of adjacent buildings, drastic tapering of columns in the upper stories, and more generally to the dynamics of the structural response.

January 17, 1995, Magnitude 6.9 Kobe Earthquake, Japan

The Kobe earthquake occurred exactly one year following the Northridge earthquake. Kobe had many welded steel moment frame buildings ranging from lowrise buildings constructed in the 1950s and 1960s to modern highrise structures constructed within the preceding 10 years. While the design and construction of these buildings are significantly different from that in the US, the extent of damage observed in steel structures in this earthquake once again point to the possibility of a set of unfortunate factors leading to disastrous consequences. Out of 630 modern steel buildings in the heavily shaken area, the Building Research Institute determined that approximately one-third experienced no significant damage, one-third relatively minor damage, and the remaining third severe damage, including partial or total collapses of approximately half of these buildings (FEMA 2000b; FEMA 2000d). When we view this in the context of the fact that the Japanese code prevalent in 1994 required 20-story steel moment frame buildings to be designed for more than 2.5 times the force levels prescribed by the 1994 Uniform Building Code (Hall 1997), we can conclude that we should expect significant damage to occur even in southern Californian steel frame buildings in the event of a large earthquake on the San Andreas fault.

Figure 4: Fractures observed in beam-to-column connections during the 1994 Northridge earthquake (Source: FEMA-355E): [A] Fracture at the fused zone; [B] Column flange "divot" fracture; [C] Fracture through column flange; [D] Fracture progresses through column web; and [E] Vertical fracture through beam shear plate connection.

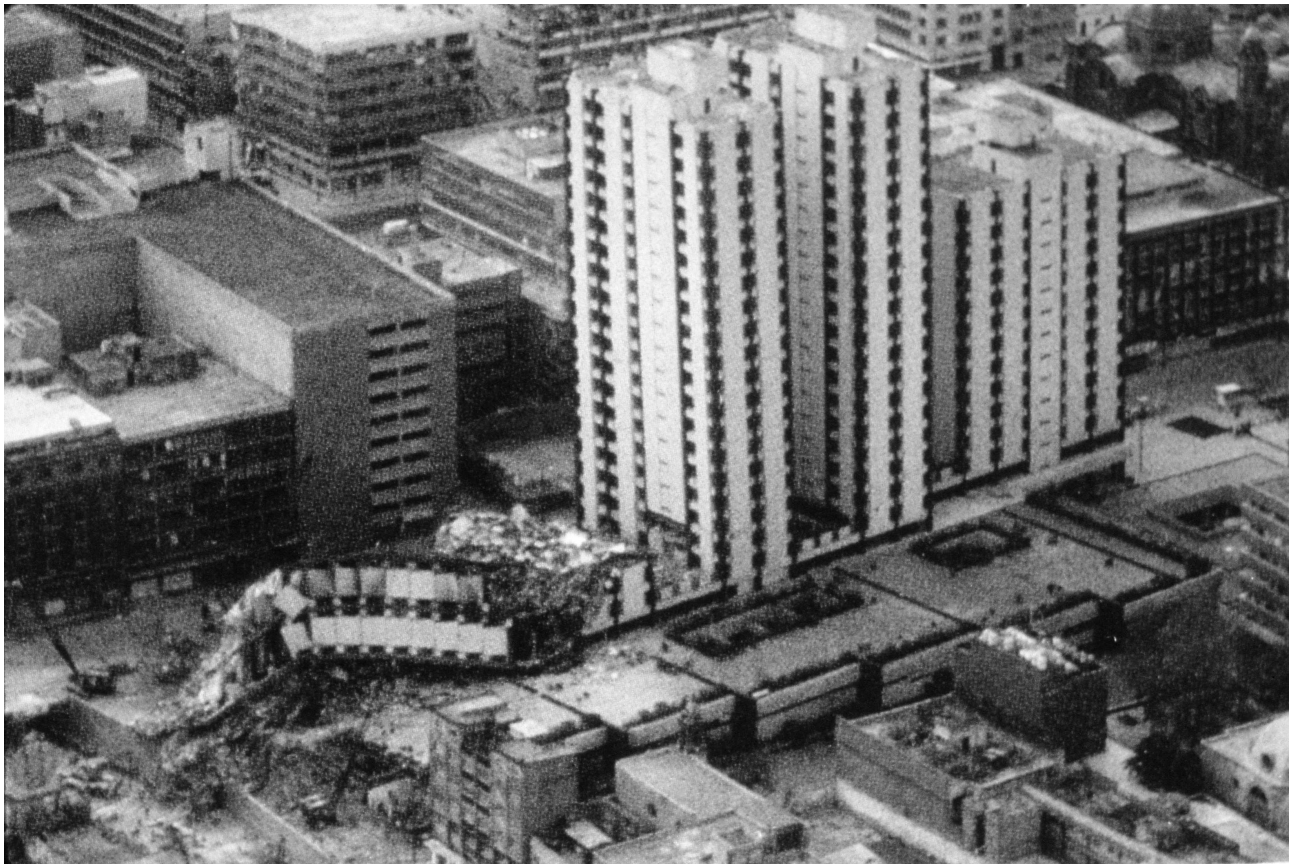

[A]

[B]

[C]

Figure 5: Mexico City Earthquake, September 19, 1985: [A] Collapse of a 21-story building on top of a 14-story building in the Pino Suarez complex. Three towers are left standing with extensive damage to the two 21-story towers. Source: Bob Reitherman; [B] Failure in the welds connecting the flanges and webs of built-up box column possibly led to local flange-buckling of the column and eventual collapse. Source: Bob Reitherman; [C] Debris of tower collapse spilled on to the streets. Source: Mehmet Celebi, USGS.

[A]

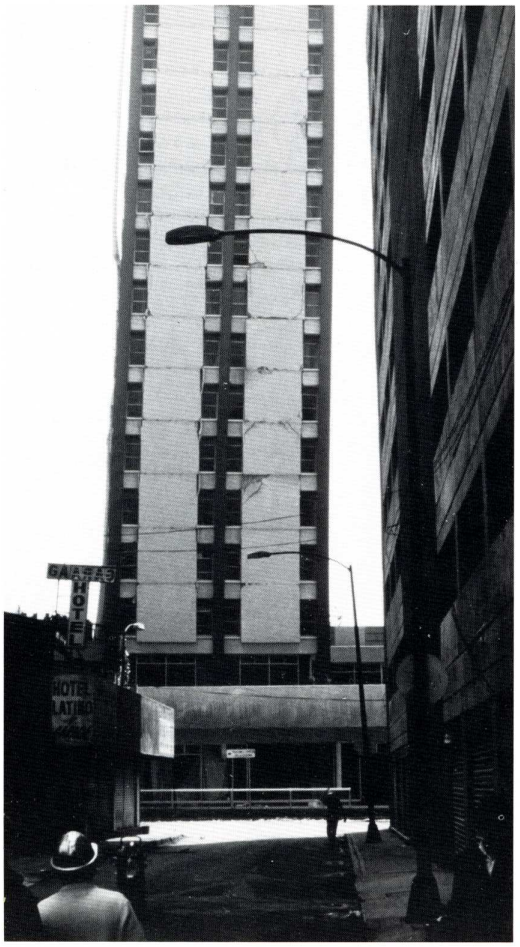

[B]

Figure 6: Mexico City Earthquake, September 19, 1985: [A] Wreckage of a 21-story steel building in the Pino Suarez Apartment Complex (Source: Mehmet Celebi, USGS); and [B] A second 21-story steel building in the same complex remained standing, but was leaning six feet out of plumb at the roof level due to yielding that resulted in a permanent interstory drift (Source: Jim Beck, Caltech). Such permanent tilting following an earthquake would most likely render the vertical transportation system (elevators) unusable due to misalignment. In addition, doors to staircase shafts may be jammed due to deformation of the frames, possibly hampering evacuation efforts.

NONLINEAR ANALYSIS OF STRUCTURAL MODELS

It is clear from the preceding discussion that any earthquake drill in the Los Angeles region should consider the possibility of serious damage to tall steel buildings, even collapses in some instances. To quantify the expected damage in a scenario event such as the shakeout earthquake, one should ideally analyze realistic models of a large number of existing buildings. Owing to the difficulty in acquiring structural design plans of existing buildings, we have limited our analyses to one existing 18-story steel moment frame building, designed according to the 1982 Uniform Building Code (UBC), that experienced significant damage (moment-frame connection fractures) during the 1994 Northridge earthquake, and two buildings designed according to the 1997 UBC, one with the same architecture as the 18-story building, and another that is 19-storied and L-shaped, and hence deemed "irregular" by the code. The L-shaped building 3 has been designed for a lateral force level that is approximately 10% larger than that for building 2. We have subjected computer models of these three buildings to the 3-component ground motion waveforms simulated by Graves.

Description of buildings

Building 1 is located within five miles of the epicenter of the 1994 Northridge earthquake. It was designed in 1984 according to the lateral force requirements of the 1982 UBC (ICBO 1982) and construction was completed in 1986-87. It has 17 office stories above ground and a mechanical penthouse on top (Figure 7). There is a single basement. The height of the building above ground is 75.7 m (248' 4") with a typical story height of 3.96 m (13' 0") and taller first, seventeenth, and penthouse stories. The plan configuration of the building is fairly uniform over its height. The lateral force-resisting system consists of two-bay welded steel moment-frames, two apiece in either principal direction of the building. There are a few setbacks in the building that do not affect the lateral force-resisting system significantly. The east, west, and south moment-frames lie on the perimeter of the building, while the north frame is located one bay inside of the perimeter. This gives rise to some torsional eccentricity. Many moment-frame beam-column connections in the building fractured during the Northridge earthquake, and the building has been extensively investigated since then by many engineering research groups (SAC 1995; Carlson 1999). Figure 7[A] shows an isometric view of a structural model of the building. A typical floor plan is given in Figure 7[D]. Detailed floor plans, beam and column sizes, and gravity, wind, and seismic loading criteria are given in Krishnan et al. (2005). A36 steel with nominal yield strength of 248.29 MPa (36 ksi) is used for all beams, while A572 Grade 50 steel with nominal yield strength of 344.85 MPa (50 ksi) is used for all columns. The floors consist of lightweight concrete slab on metal deck supported by steel beams and girders framing into gravity and moment-frame columns. The three largest computed natural periods of the building are 4.43s (X translation), 4.22s (Y translation), and 2.47s (Z rotation).

Building 2 is similar to building 1, but the lateral force-resisting system has been redesigned according to the 1997 UBC (ICBO 1997). The fundamental difference between the two structures is that the new building has been designed for larger earthquake forces (accounting for near-source effects) and stringent redundancy requirements in the lateral force-resisting system. This leads to significantly different dynamic characteristics. In general, the redesigned building can be expected to perform better than the existing building in the event of an earthquake. The gravity and wind loading criteria from the existing building were retained for the design of the new building. For the seismic static base shear calculation, near-source factors were computed assuming a Type A seismic source at a distance of 5 km from the building; soil type S_b was assumed as well (ICBO 1997). The stricter lateral force and redundancy requirements of UBC97 led to a reconfiguration of the lateral system resulting in a greater number of bays of moment-frames in each direction (8 bays in each direction, although the three-bay moment frames shown in the typical floor plan in Figure 7[E] dominate over the

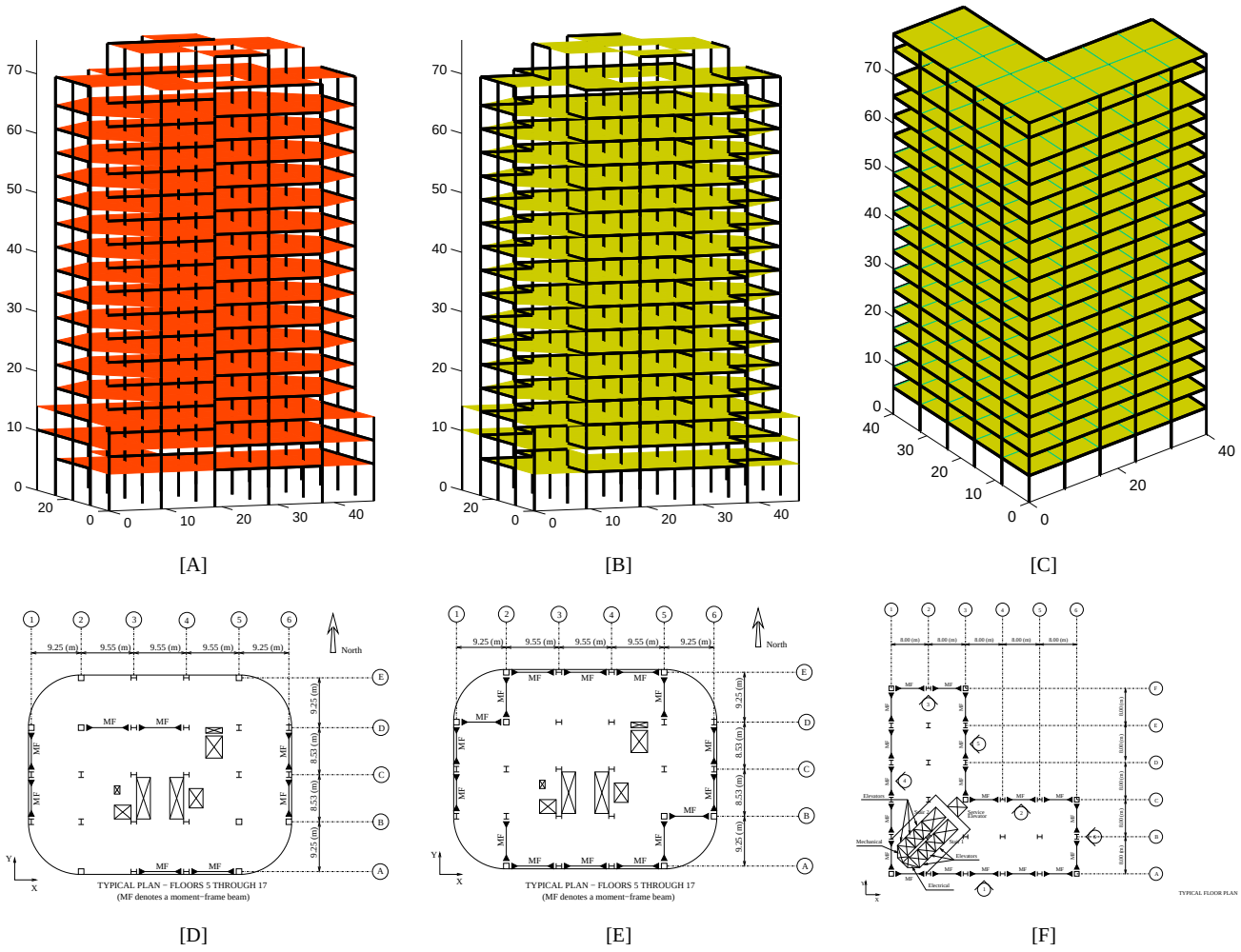

Figure 7: San Andreas fault shakeout scenario earthquake simulation: Structural models of three buildings are analyzed. Building 1 is a model of an existing 18-story office building in Woodland Hills designed using the 1982 Uniform Building Code (UBC) and completed in 1984. Building 2 represents a modern version of building 1, designed according to the 1997 UBC. The third model is that of an L-shaped irregular 19-story office building also designed according to the 1997 UBC. Schematics of the three models are shown in [A], [B], and [C], respectively and the corresponding typical floor plans are shown in [D], [E], and [F], respectively.

single-bay moment frames). Detailed floor plans, beam and column sizes, and the gravity, wind and seismic loading criteria are given in Krishnan et al. (2005). Note that the moment-frame that was located in the interior of the existing building on grid D has been moved to the perimeter (to grid E). The two-story space required at the lobby of the building precludes moment-frame beams on grid E at the second floor between grids 1–2, 3–4, and 4–5. This probably prompted the structural engineers of the existing building to move the frame to the interior of the building to grid D. But since the stiffness demand at the lower levels is not as high, it was concluded that the frame would be stiff enough with a single beam at the second floor on grid E. Box-sections are used for the columns left unsupported laterally for two stories at E-1, E-4, E-5, and E-6, to keep the slenderness ratio governing the design within reasonable limits. ASTM A572 Grade 50 steel with nominal yield

strength of 344.85 MPa (50 ksi) is used for both beam and column sections, as well as for doubler plates that are provided to strengthen panel zones. The three largest computed natural periods of the building are 3.72s (X translation), 3.51s (Y translation), and 2.24s (Z rotation).

Building 3 is L-shaped in plan (Figure 7[F]) with one elevator core serving both wings of the building. In L-shaped buildings such as this the wings, with fewer moment-frame bays, being less stiff have a tendency to flap during strong shaking. Out-of-phase shaking of the wings could lead to stress concentration at the reentrant corner and potential failure in a tearing mode. In-phase shaking of the wings could lead to twisting in the building and potential failure in a torsional mode. The UBC classifies such buildings as irregular and stipulates that they be designed for lateral forces that are approximately 10% larger than those prescribed for regular buildings. Typical story height of this structure is 4.0 m with variations at the lobby and the mechanical stories. The isometric view of the building is illustrated in Figure 7[C]. The wings have only two-bay moment frames across their ends and, as a result, are softer than the spine (reentrant corner region) of the building. Wind forces control the design of the moment-frames at the wings. The center of stiffness (on plan) of the building being closer to the reentrant corner than to the point of application of wind forces leads to twisting in the building under wind forces. Since the wings are soft, this torsion leads to large drifts at the far corners (at grid intersections F-1, F-3, C-6 and A-6 in Figure 7[F]). While reduction in the drift due to building translation (sway) is achieved by stiffening all moment-frames, reducing the drift in the short direction of the wings requires the stiffening of the beams and columns in the 2-bay moment-frames at the wings (frames 3 and 6 along grids F and 6 in Figure 7[C]) relative to those in the 3-bay and 5-bay moment-frames (frames 1, 2, 4 and 5 along grids 1, 3, A and C, respectively). This moves the center of stiffness from within the spine to a location very close to the reentrant corner. However, this remedial measure to distribute the stiffness (on plan) more uniformly is still not sufficient to eliminate twisting in the building under wind forces. But the reduction in the translational drift (sway) allows the wind drift at the far corners (at grid intersections F-1, F-3, C-6, and A-6 in Figure 7[C]) to be limited to 0.0025. The three largest computed natural periods of the building are 3.39s (X+Y+ translation), 3.32s (X-Y+ translation), and 2.33s (Z rotation). Greater details of this building can be found in Krishnan (2003b, 2007).

Analysis program FRAME3D

The nonlinear damage analyses of the structures are performed using the program FRAME3D (Krishnan 2003a). FRAME3D (http://www.frame3d.caltech.edu) utilizes a Newton-Raphson iteration strategy applied to an implicit Newmark time integration scheme to solve the nonlinear equations of motion at each time step. It utilizes a corotational formulation to incorporate geometric nonlinearity, which enables the modeling of the global stability of the building, accounting for $P-\Delta$ effects accurately. The moment-frame beams are modeled using elastofiber elements that consist of three segments, two nonlinear end segments that are subdivided in the cross-section into a number of fibers, and an interior elastic segment (Krishnan and Hall 2006b), while the columns are modeled using 5-segment modified elastofiber elements consisting of a middle nonlinear segment, in addition to the two end nonlinear segments, with two elastic segments sandwiched between the nonlinear segments. The middle nonlinear segment enables the modeling of column buckling. The beam-to-column joints are modeled in three dimensions using FRAME3D panel zone elements while the gravity columns are modeled using plastic hinge elements (Krishnan and Hall 2006a). These elements have been shown to simulate damage accurately and efficiently (Krishnan 2003b). Material nonlinearity resulting in flexural yielding, strain-hardening and ultimately rupturing of steel at the ends of beams and columns, and shear yielding in the joints (panel-zones) is included. The fracture mode of failure is included in connections, however, local flange buckling in beams and columns is not. It is assumed that a fiber that is fractured cannot resist tension but, upon contact, can start resisting compression again. Column splices can be incor-

porated into the model but are excluded in this study. Floor-framing beams with shear connections used to support gravity loads are not modeled. Their contribution to the strength and stiffness of the building may not be negligible. Soil-structure interaction (SSI, e.g., Trifunac et al. 2001; Stewart et al. 1998) is not included in the analyses because the required soil information pertaining to each site is not available.

Modeling the susceptibility to fracture of the beam-to-column connections

There is great uncertainty in the performance of the beam-to-column connections in welded steel moment frame buildings as evidenced in the Northridge earthquake. To encompass the broad spectrum of beam-to-column connection behavior, two models are considered for each building, one with perfect connections, and the other with susceptible connections. The specifications (FEMA 2000c) developed by the Federal Emergency Management Agency (FEMA) for moment-frame construction following the Northridge earthquake should result in superior connection performance, and hence, the connections in the buildings designed according to UBC97 are assumed to be less vulnerable to fracture than for the older building 1. For building 1, the fracture strain for the fibers in the bottom-flanges of moment frame beams is drawn from the distribution shown in Figure 8[A] (with a 20% probability that the fracture strain is 0.9 ϵ_y; 20% probability that it is 2 ϵ_y; 20% probability that it is 5 ϵ_y; 20% probability that it is 15 ϵ_y; and 20% probability that it is 40 ϵ_y), while that for the top-flanges and the webs of the beams is drawn from the distribution shown in Figure 8[B] (with a 30% probability that the fracture strain is 10 ϵ_y; 30% probability that it is 20 ϵ_y; 20% probability that it is 40 ϵ_y; and 20% probability that it is 80 ϵ_y). For column flange and web fibers, it is assumed that the fracture strains are far greater than the rupture strain, thus precluding the occurrence of fractures.

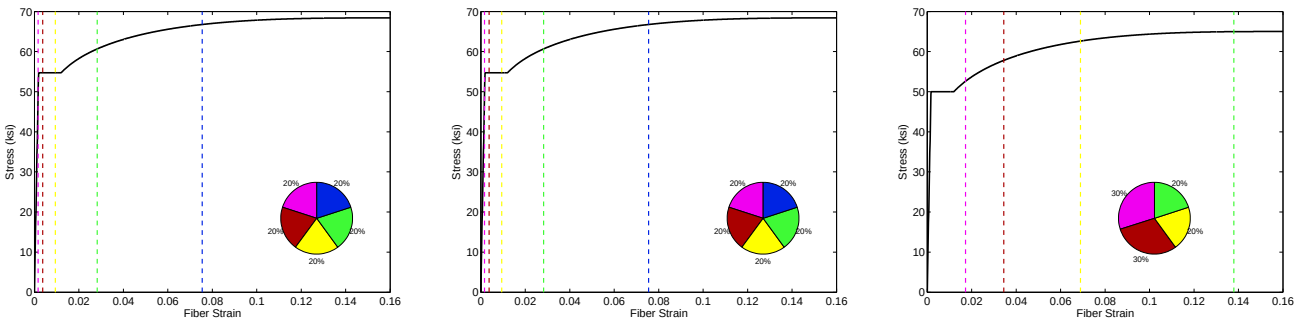

[A] [B] [C]

Figure 8: Marked on the backbone axial stress-strain curves of the elastofiber element fibers is the distribution of fracture strain assumed for the susceptible connection case of building 1 ([A] beam bottom flange, and [B] beam web and top flange) and buildings 2 & 3 ([C] beam bottom flange only). The pie chart shows the probability of attaining each of the five fracture strains marked on the backbone curve, for e.g., in [A] there is a 20% chance that the fiber fracture strain is about 0.028 as indicated by the green dashed line and the green colored pie in the pie chart.

For the susceptible connection cases of buildings 2 and 3, it is assumed that the fracture strain for all fibers (top and bottom flanges, as well as the web) is drawn from the distribution shown in Figure 8[C], which is the same as that used for the top-flanges of the moment frame beams in building 1. The difference in the actual values of the fracture strain are due to differences in the yield strains of the steel used in the two types of buildings. It should be noted that the lack of a sufficiently large data set on fractured connections, combined with the great variety of factors affecting the behavior of beam-to-column connections, means that the probability distributions assumed in this study are not very reliable, and as-built connections may either be more or less vulnerable to fracture.

Orientation of the building models

For each building, two orientations are investigated. The base orientation of all models is with the positive X axis pointing to the geographic East direction and the positive Y axis pointing to the North direction. The alternate rotated orientation for buildings 1 and 2 consists of rotating the buildings 90 degrees counter-clockwise, such that the positive X axis points to the North direction and the positive Y axis points to the West direction. The two wings of the L-shaped building are identical to each other and rotating the model by 90 degrees would not change the results. However, rotating the building by 45 degrees will result in a different angle of attack in as far as the ground motion is concerned and could yield significantly different results. Hence, the rotated configuration for building 3 consists of a 45 degree counter-clockwise rotation from the base orientation.

Assessing building damage

The primary structural response parameter that is used to evaluate structural performance is the peak interstory drift, which is the difference in displacement between the top and bottom of a story normalized by its height. The peak interstory drift is a good indicator of how far the building is from $P-\Delta$ instability and collapse. It is also closely related to the plastic rotation demand on individual beam-column connection assemblies, i.e., the greater the yielding in the beams, columns and joints, the greater this interstory drift would be, reducing the stability of the building.

Since there is very little usable data to assess the performance of tall buildings based on calculated drifts, we take an empirical approach proposed by the Federal Emergency Management Agency (FEMA). For the rehabilitation of existing buildings, FEMA 356 (FEMA 2000a) defines three performance levels: Immediate Occupancy (IO) refers to a post-earthquake damage state in which very limited structural damage has occurred. The risk of life-threatening injury as a result of structural damage is very low, and although some minor structural repairs may be appropriate, these would generally not be required prior to reoccupancy. Life Safety (LS) is a post-earthquake damage state that includes damage to structural components but retains a margin against onset of partial or total collapse. Collapse Prevention (CP) refers to a post-earthquake damage state that includes damage to structural components such that the structure continues to support gravity loads but retains no margin against collapse. For existing buildings, the interstory drift limits for the IO, LS, and CP performance levels specified by FEMA are 0.007, 0.025, and 0.05, respectively.

Based on these criteria, we will assume that the buildings will be red-tagged if the peak interstory drift ratios exceed 0.05. If the peak interstory drift ratio exceeds 0.075 we will assume that the building has collapsed.

Building performance

A total of 9408 3-D nonlinear time-history analyses (784 analysis sites x 3 buildings x 2 orientations x 2 connection fracture susceptibility models) were performed using FRAME3D on 300 processors in two high-performance computing clusters at Caltech. In each case, detailed structural damage as well as displacement and drift estimates over the height of the building were determined. Figure 9 shows maps of peak interstory drift ratios in the three buildings assuming susceptible connections (Figures 9[A], 9[C], and 9[E]), and perfect connections (Figures 9[B], 9[D], and 9[F]). The color-coding on the maps follows the FEMA performance criteria described previously, with blue color areas representing buildings that have performed the best and can likely be immediately occupied following the earthquake (IO performance level), green color regions representing some damage resulting in business interruption but no loss of life (LS performance level), yellow color regions reflecting damage serious enough to cause loss of life, but not enough to cause collapse, red color regions reflecting severe damage with a great risk of collapsing requiring the structure to be red-tagged, and finally pink color

regions representing regions where the structures can be considered to have collapsed. Building 1 which was designed according to the 1982 UBC exhibits the worst performance with the susceptible connection model collapsing at 18.3% of the 784 analysis sites and being red-tagged at 11.7% of the sites. The L-shaped building 3 performs the best with the percentage of collapsed and red-tagged instances being 10.3% and 6.4%, respectively. The performance of building 2 is only slightly worse than building 3. If we assume that the beam-to-column connections are perfect, then there is a significant drop in the number of collapsed and red-tagged buildings, for e.g., for building 1 the percentage of collapsed instances is 7.0%, while the percentage of red-tagged instances is 11.9%. The performance of the buildings is summarized in Table 1.

The results for the rotated cases for each of the three buildings with perfect and susceptible connections are summarized on peak interstory drift ratio maps in Figure 10. The rotated orientation is detrimental to buildings 1 and 2 with a 2-4% increase in the percentage of collapses. Notably, downtown Los Angeles with the greatest concentration of high-rise buildings, and hence the location with the greatest likelihood of existence of steel moment frame buildings of this class, falls in the red-tagged zone for the susceptible connection case of building 1. There is a slight improvement in the performance of the rotated L-shaped building 3 with a 1.5% drop in the percentage of red-tagged instances.

Shown in Figure 11 are the maps of the average peak interstory drift ratios in each of the three buildings for the four cases (base and rotated orientations, and susceptible & perfect connections). It is clear once again from these maps that on the average, building 1 performs the worst, while the more modern building 3 performs the best. In all three cases, downtown Los Angeles falls within 5-10 km of the red-tagged zone. Figure 12 depicts the collapse of the building 1 model located at Baldwin Park in the base orientation with susceptible beam-to-column connections. The large drifts in stories 4-7 leads to instability and collapse of the upper stories. The dead weight of the upper stories collapsing could lead to the entire building turning to rubble.

Table 1: Performance of the three buildings in the base and rotated orientations, as well as with susceptible and perfect beam-to-column connections. Numbers indicate the percentage out of 784 analysis sites at which the performance of the model can be categorized as: (a) immediately occupiable (IO) following the earthquake; (b) life-safe (LS), with visible damage requiring repairs and building closure, but no loss of life; (c) collapse is prevented (CP), but with significant damage resulting in loss of lives; (d) red-tagged (RT) as a result of major damage and possibly on the verge of collapse; or (e) collapsed (CO).

Building	**Orientation**	**Fracture Susceptibility**	**Performance Level**				
			IO (blue)	**LS (green)**	**CP (yellow)**	**RT (red)**	**CO (Pink)**
Building 1 (1982 UBC)	Base	Susceptible	5.2	28.3	36.5	11.7	18.3
		Perfect	5.4	29.7	46.0	11.9	7.0
	Rotated	Susceptible	4.8	29.7	33.8	7.5	24.2
		Perfect	4.9	31.0	42.2	10.7	11.3
Building 2 (1997 UBC)	Base	Susceptible	8.5	36.4	35.5	9.8	9.8
		Perfect	8.5	37.2	42.0	7.7	4.7
	Rotated	Susceptible	7.7	36.0	36.0	8.2	12.1
		Perfect	7.7	37.4	41.2	10.0	3.8
Building 3 (1997 UBC) (L-Shaped)	Base	Susceptible	8.2	42.4	39.0	6.6	3.9
		Perfect	8.2	42.8	40.9	6.6	1.5
	Rotated	Susceptible	9.9	45.5	34.2	4.6	5.7
		Perfect	9.9	46.0	35.9	5.5	2.7

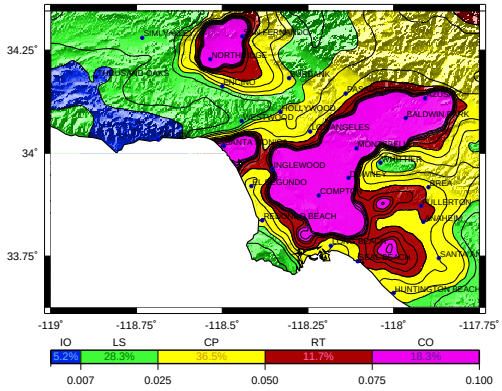

[A]

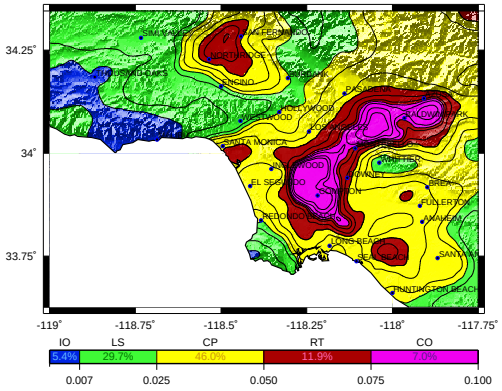

[B]

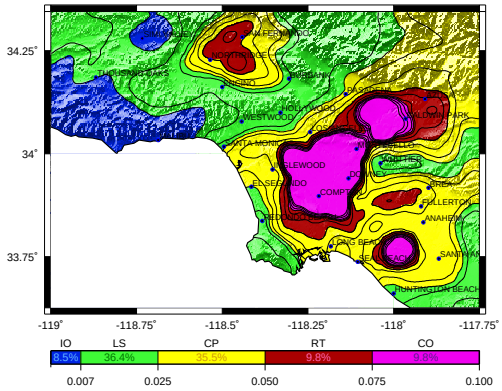

[C]

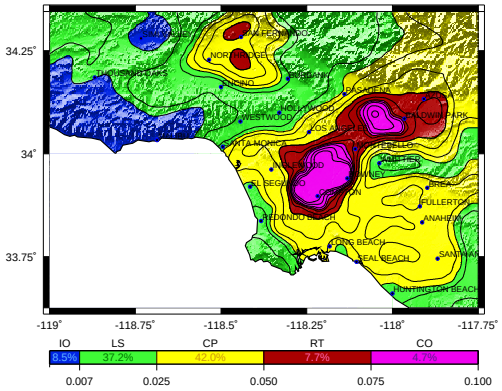

[D]

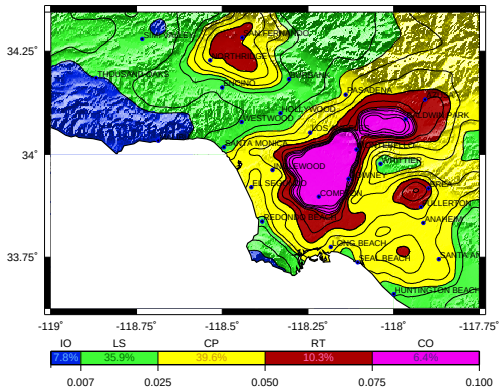

[E]

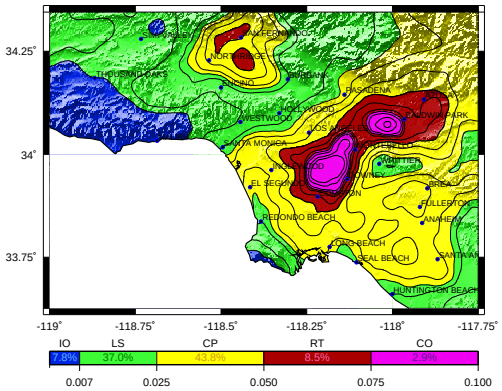

[F]

Figure 9: Maps of peak interstory drift ratios of models of the three buildings placed in the base orientation. For each building two cases are considered one with perfect connections ([B], [D], and [F] for buildings 1, 2, and 3, respectively), and the other with susceptible connections ([A], [C], and [E] for buildings 1, 2, and 3, respectively). The numbers in the color bar represent the instances in each of the 5 performance categories as a percentage of the total number of analysis sites (784). IO (blue): Immediately occupiable after the earthquake; LS(green): Visible damage, but no loss of life; repairs may require building closure; CP (yellow): Heavy damage with loss of life, but collapse is prevented; RT (red): Severely damaged and on the verge of collapse; red-tagged; CO (pink): Collapsed.

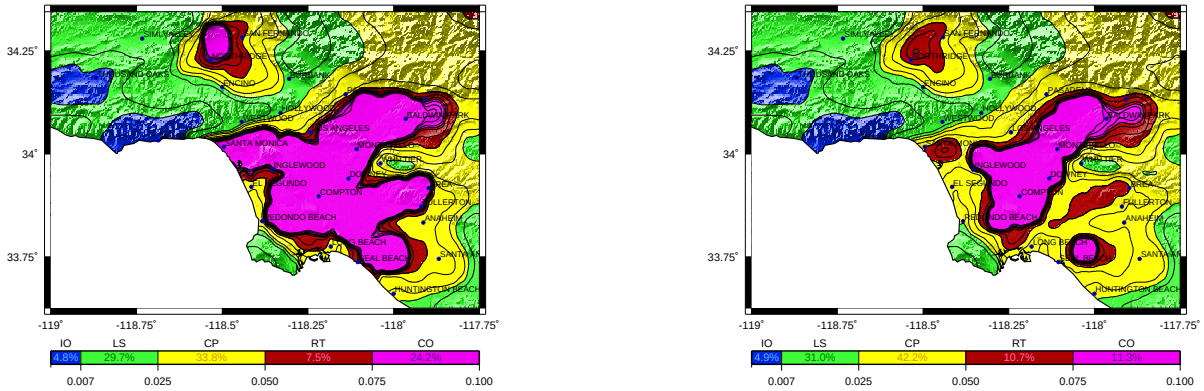

[A]

[B]

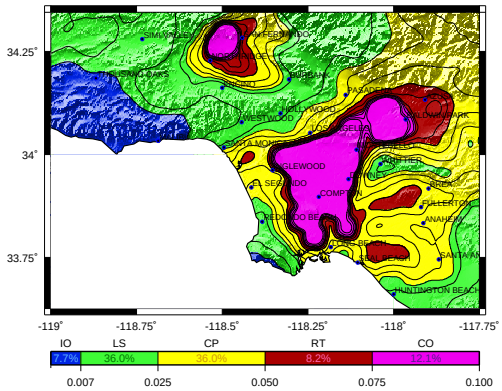

[C]

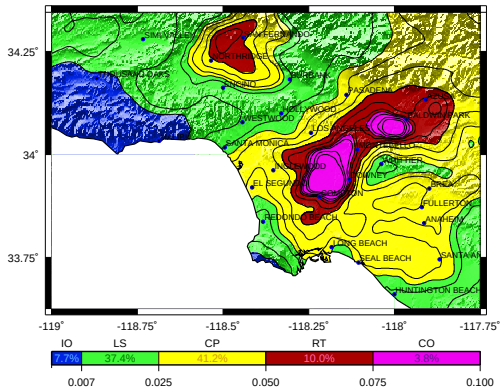

[D]

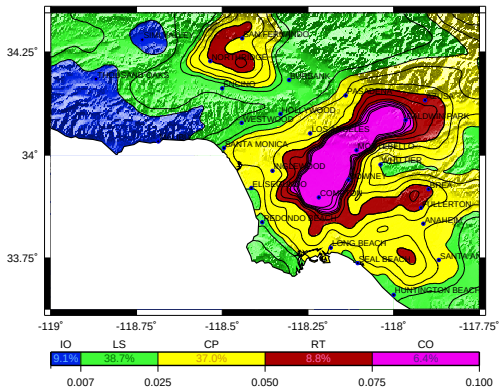

[E]

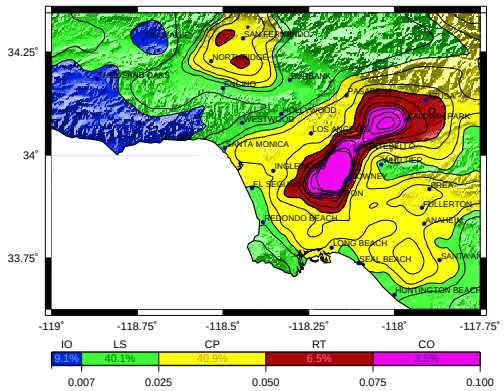

[F]

Figure 10: Maps of peak interstory drift ratios of models of the three buildings, with buildings 1 and 2 oriented 90° counter-clockwise to the base orientation, and the L-shaped building 3 oriented 45° counter-clockwise to the base orientation. [B], [D], and [F]: Buildings 1, 2, and 3, respectively, with perfect beam-to-column connections; [A], [C], and [E]: Buildings 1, 2, and 3, respectively, with susceptible connections. The numbers in the color bar represent the instances in each of the 5 performance categories as a percentage of the total number of analysis sites (784).

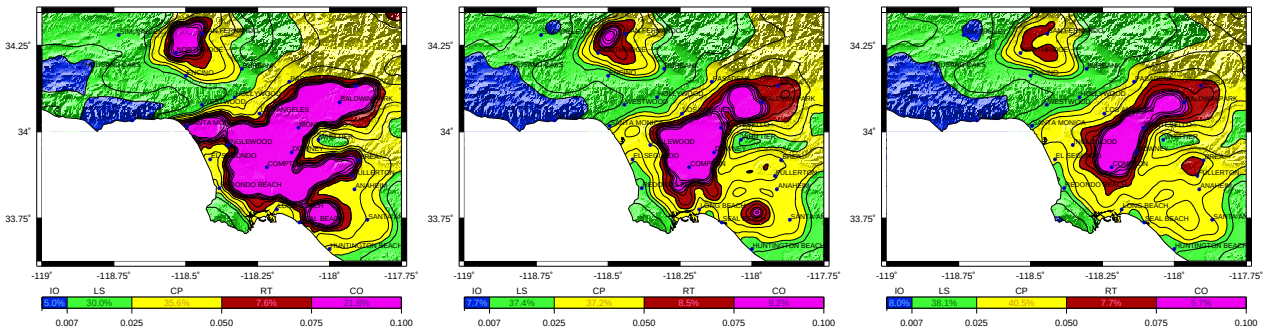

[A] [B] [C]

Figure 11: Maps of average peak interstory drift ratios of models of the three buildings ([A], [B], and [C] for buildings 1, 2, and 3, respectively). Responses of four models (2 orientations x 2 connection susceptibility assumptions have been averaged for each building.

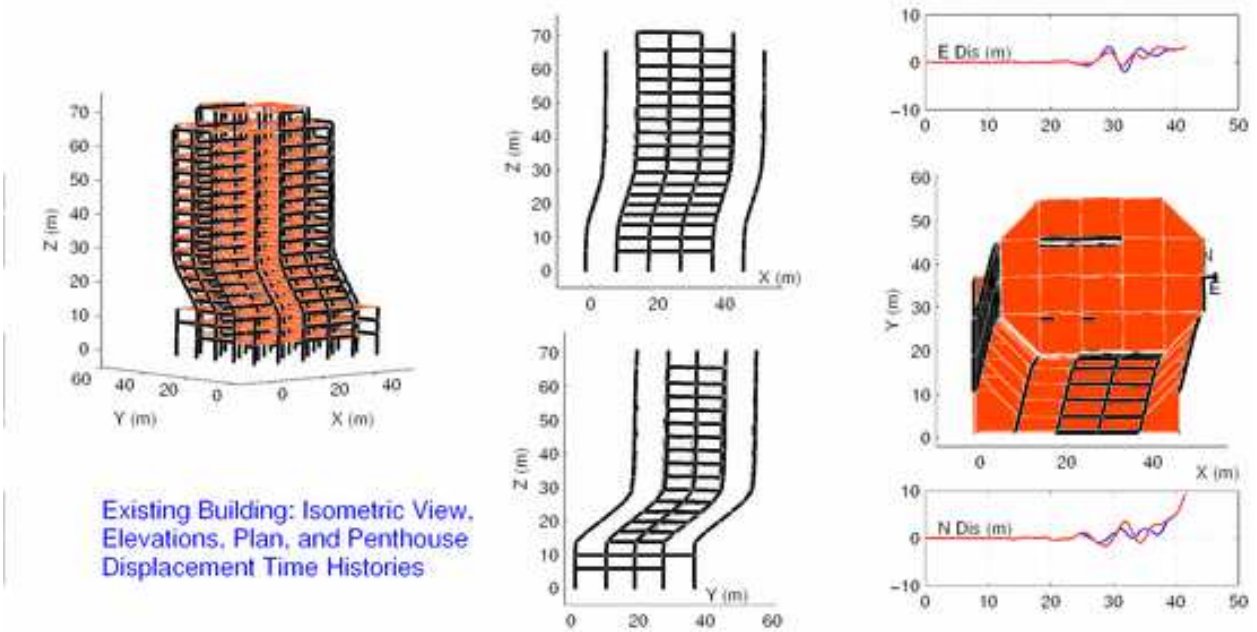

Figure 12: Snapshot of the response of the susceptible connection model of building 1, located at Baldwin Park with base orientation, at the initiation of collapse. The displacements are scaled by a factor of 2 for better visualization of the collapse mechanism.

SHAKEOUT EXERCISE: HOPE FOR THE BEST, PREPARE FOR THE WORST

The location of tall buildings in the Los Angeles metropolitan area with 10 or more stories is shown in Figure 13. The buildings are clustered in small pockets that are aligned with the major freeways in the region. Most tall buildings have been built along Interstate freeway I-10 from Santa Monica to downtown Los Angeles, in the mid-Wilshire district along Wilshire boulevard, and along State Highway 101 from Hollywood to Canoga Park in the San Fernando valley. In addition a few tall buildings are located along Interstate freeways, I-5 and I-405. The 14 locations where highrise buildings are concentrated are Canoga Park, Encino, Santa Monica, Century City, Universal City, Park La Brea, Hollywood, Glendale, El Segundo, downtown Los Angeles, Pasadena, Long Beach, Santa Ana-Anaheim corridor, and Irvine. There are a few solitary towers scattered across the region, but for the purposes of the shakeout exercise close attention may be paid to these 14 tall building clusters, with the exception of those single towers that are located quite close to the fault. The size of circles shown in the figure is proportional to the number of stories. There are 489 buildings with 10-19 stories, 118 buildings with 20-29 stories, 28 buildings with 30-39 stories, 11 buildings with 40-49 stories, and 10 buildings with 50 or more stories. Many more are in the planning stages or under construction. Its clear that majority (607) are in the 10-30 story range. Typical lateral force-resisting systems for structures in this height range are steel moment frames, steel braced frames, concrete moment frames, and concrete shear wall systems. In the 25-30 story range, dual systems comprising of a combination of perimeter steel moment frames and braced frame core, or perimeter concrete moment frames and shear wall core may have been utilized. Nevertheless, we could assume that about one-quarter of the 607 buildings in the 10-29 story category consist of steel moment frames as their primary lateral force resisting system, similar to the buildings considered in this study.

The map of the average peak interstory drift ratios for all 12 analysis cases is depicted in Figure 14. On the average, Canoga Park, Encino, Universal City, Hollywood, and Irvine fall in the green zone, indicating visible damage with business interruption, but no loss of life. Santa Monica, Century City, Park La Brea, Glendale, El Segundo, downtown Los Angeles, Pasadena, Long Beach and the Santa Ana-Anaheim corridor fall in the yellow zone, indicating damage serious enough to cause loss of life, but collapse is prevented. Having said this, almost all the locations that occur in the yellow zone are within 10 km of the red and pink zones. What this means is that given a different set of earthquake source parameters, it is entirely possible that at least some of these locations may end up in the red or pink zones indicating collapses or the need for red-tagging. For example, in a previous simulation of the repeat of an 1857-like magnitude 7.9 earthquake on the San Andreas fault with rupture initiating in Parkfield in central California and propagating down south a distance of 290 km, the building 1 model when located in the San Fernando valley collapsed at most locations including Canoga Park and Encino as shown in Figure 15. This simulation used a different source model (inferred from the November 3, 2002 Denali fault earthquake) and velocity model (the Harvard-LA or SCEC CVM-H model) for the ground motion simulation. The differences in the hypocenter location, slip distribution, rupture directivity, and the velocity model result in a dramatically different distribution of building damage. Bearing this in mind, it is our recommendation that the shakeout drill be planned with a damage scenario comprising of 5% of the estimated 150 steel moment frame structures in the 10-30 story range collapsing (8 collapses), 10% of the structures red-tagged (16 red-tagged buildings), 15% of the structures with damage serious enough to cause loss of life (24 buildings in the yellow zone with fatalities), and 20% of the structures with visible damage requiring building closure (32 buildings with visible damage and possible injuries). Note that these estimates are for steel moment frame buildings only. We recommend that similar analyses be done for buildings utilizing other lateral force-resisting systems mentioned previously. In the absence of such analysis, we recommend that the shakeout drill be conducted assuming a similar percentage of collapses and red-tags for other types of buildings as well. Distinction has not been made here between residential structures and office buildings. Since the occupancy at the time of the earthquake

depends upon the time of the day and the type of structure, these two factors may have a significant impact on the eventual outcome, in as far casualties are concerned. Emergency response strategies must take these factors into account along with consideration to power outages, gas leak-initiated fires, and failure of transportation networks. For the yellow-zone and red-tagged tall buildings, emergency response units should plan for the misalignment of elevators rendering them non-operational, as well as the blocking of exit routes due to debris, jamming of doors to stair shafts, etc. Smoke and dust may result in zero/low visibility as well as make it impossible to breathe. In such cases, aerial and/or ladder evacuation may have to be undertaken.

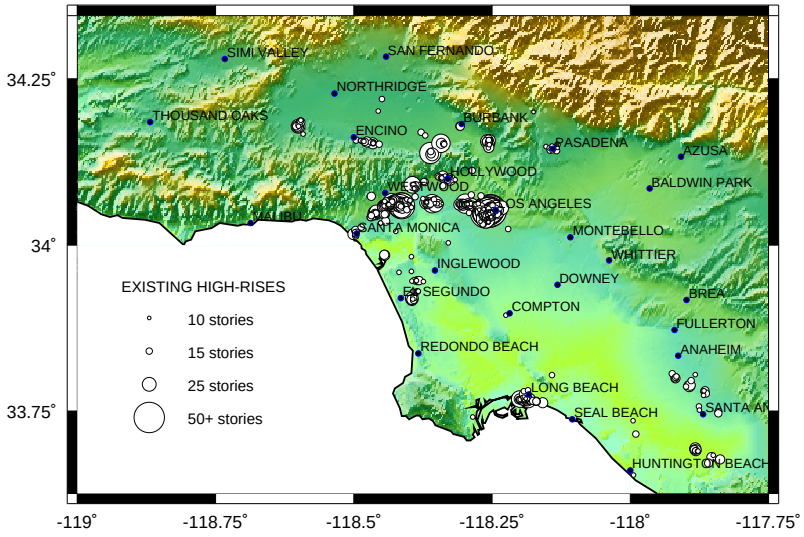

Figure 13: Distribution of tall buildings (10 stories or greater) in the Los Angeles metropolitan area as of mid-2007. There are 489 buildings with 10-19 stories, 118 buildings with 20-29 stories, 28 buildings with 30-39 stories, 11 buildings with 40-49 stories, and 10 buildings with 50 or more stories. Data source: Emporis.com by way of Keith Porter, University of Colorado at Boulder

ACKNOWLEDGEMENTS

This study was supported in part by a USGS Multi-Hazards Demonstration Project grant. The source model for the shakeout scenario earthquake was generated by Brad Aagaard (USGS), Ken Hudnut (USGS), and Rob Graves (URS Corporation) in consultation with the SCEC community, while the ground motion simulations were performed by Rob Graves. The numerical simulations were performed in part on the CITerra, a high-performance computing cluster (HPCC) hosted by the Division of Geological and Planetary Sciences at the California Institute of Technology, and GARUDA, an HPCC dedicated for end-to-end simulations hosted within the Civil Engineering department at Caltech. The purchase and installation of GARUDA were made possible in large part by the Ruth Haskell Research Fund, the Tomiyasu Discovery Fund, and Dell Inc.

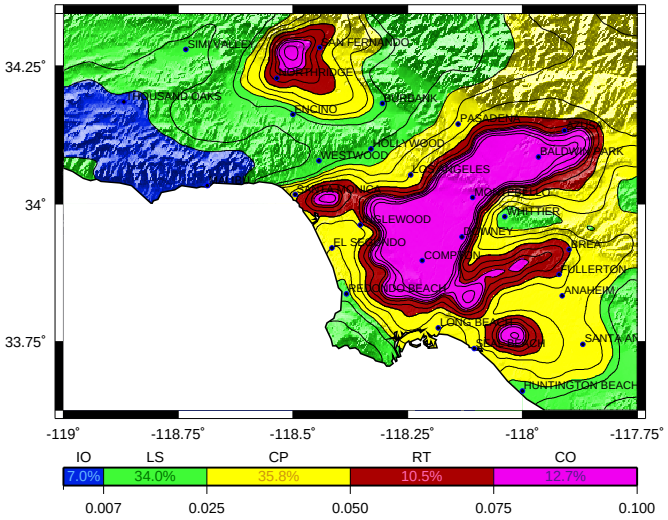

Figure 14: Map of average peak interstory drift ratios for the 12 structural models considered in this study (3 buildings x 2 orientations x 2 connection susceptibility assumptions). Structural models hypothetically located at 784 analysis sites spread across the Los Angeles basin have been analyzed. 7% of these can be immediately occupied after the earthquake (blue zone); 34% will have damage requiring building closure, but no loss of life (green zone); 35.8% will have serious damage resulting in loss of life, but collapse is prevented (yellow zone); 10.5% will have to be red-tagged and may be on the verge of collapse (red zone); and 12.7% will have collapsed (pink zone). Note that the actual location of existing tall buildings in the LA basin has no bearing on these results.

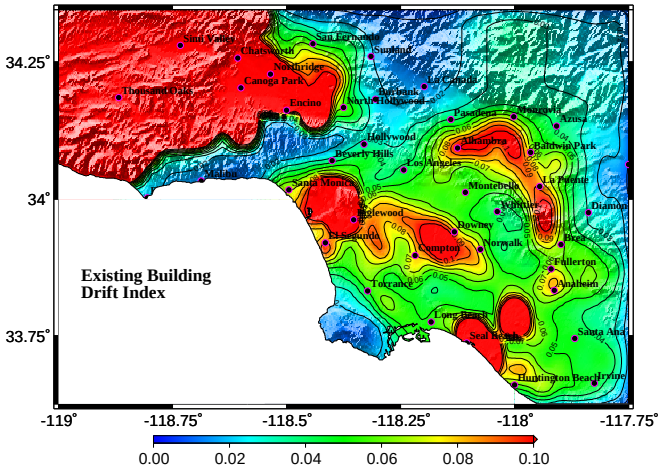

Figure 15: Map of peak interstory drift ratios in building 1 when subjected to ground motions from a simulated 1857-like magnitude 7.9 San Andreas fault earthquake with rupture initiating in Parkfield in central California and propagating a distance of about 304 km in a southeasterly direction. Note the significantly different damage distribution. This simulation, although of a similar magnitude earthquake, is rupturing a different segment of the San Andreas fault. It uses a different earthquake source model, different hypocenter location and directivity, and a different velocity model. This means that the outcome in as far as tall steel building damage is concerned may vary significantly depending upon the actual source characteristics, and we must be prepared for all possible outcomes. Note that the color scale used in this map is different from that used to summarize results from the current study.

References

Beck, J. L. and J. F. Hall (1986). Structural damage in Mexico city. *Geophysical Research Letters 13*, 589–592.

Carlson, A. (1999). Three-dimensional nonlinear inelastic analysis of steel moment frame buildings damaged by earthquake excitations. Technical Report EERL 99-02, Earthquake Engineering Research Laboratory, California Institute of Technology, Pasadena, California, USA.

FEMA (2000a). *Prestandard and Commentary for the Seismic Rehabilitation of Buildings*. FEMA-356. Federal Emergency Management Agency, USA.

FEMA (2000b). *Recommended Seismic Evaluation and Upgrade Criteria for Existing Welded Steel Moment Frame Buildings*. FEMA-351. Federal Emergency Management Agency, USA.

FEMA (2000c). *Recommended Specifications and Quality Assurance Guidelines for Steel Moment Frame Construction for Seismic Applications*. FEMA-353. Federal Emergency Management Agency, USA.

FEMA (2000d). *State of the Art Report on Past Performance of Steel Moment Frame Buildings in Earthquakes*. FEMA-355E. Federal Emergency Management Agency, USA.

Hall, J. F. (1997). Seismic response of steel frame buildings to near-source ground motions. Technical Report EERL 97-05, Earthquake Engineering Research Laboratory, California Institute of Technology, Pasadena, California.

Hudnut, K. W., L. M. Jones, and B. T. Aagaard (2007). The southern California shakeout scenario, Part 1: Earth science specification of a big one. In *Annual Meeting of the Seismological Society of America*. Abstract reference number 07-501.

ICBO (1982). *1982 Uniform Building Code*. Volume 2. International Conference of Building Officials, Whittier, California, USA.

ICBO (1997). *1997 Uniform Building Code*. Volume 2. International Conference of Building Officials, Whittier, California, USA.

Kohler, M., H. Magistrale, and R. Clayton (2003). Mantle heterogeneities and the SCEC three-dimensional seismic velocity model version 3. *Bulletin of the Seismological Society of America 93*, 757–774.

Krishnan, S. (2003a). FRAME3D – A program for three-dimensional nonlinear time-history analysis of steel buildings: User guide. Technical Report EERL 2003-03, Earthquake Engineering Research Laboratory, California Institute of Technology, Pasadena, California, USA.

Krishnan, S. (2003b). Three-dimensional nonlinear analysis of tall irregular steel buildings subject to strong ground motion. Technical Report EERL 2003-01, Earthquake Engineering Research Laboratory, California Institute of Technology, Pasadena, California, USA.

Krishnan, S. (2007). Case studies of damage to 19-storey irregular steel moment frame buildings under near-source ground motion. *Earthquake Engineering and Structural Dynamics 36*(7), 861–885.

Krishnan, S. and J. F. Hall (2006a). Modeling steel frame buildings in three dimensions – Part I: Panel zone and plastic hinge beam elements. *Journal of Engineering Mechanics 132*(4), 345–358.

Krishnan, S. and J. F. Hall (2006b). Modeling steel frame buildings in three dimensions – Part II: Elastofiber beam element and examples. *Journal of Engineering Mechanics 132*(4), 359–374.

Krishnan, S., C. Ji, D. Komatitsch, and J. Tromp (2005). Performance of 18-story steel moment frame buildings during a large San Andreas earthquake – a Southern California-wide end-to-end simulation. Technical Report EERL

2005-01, http://caltecheerl.library.caltech.edu, Earthquake Engineering Research Laboratory, California Institute of Technology, Pasadena, California, USA.

Krishnan, S., C. Ji, D. Komatitsch, and J. Tromp (2006a). Case studies of damage to tall steel moment frame buildings in southern California during large San Andreas earthquakes. *Bulletin of the Seismological Society of America 96*(4), 1523–1537.

Krishnan, S., C. Ji, D. Komatitsch, and J. Tromp (2006b). Performance of two 18-story steel moment frame buildings in southern California during two large simulated San Andreas earthquakes. *Earthquake Spectra 22*(4), 1035–1061.

Magistrale, H., S. Day, R. Clayton, and R. Graves (2000). The SCEC southern California reference three-dimensional seismic velocity model version 2. *Bulletin of the Seismological Society of America 90*(6B), S65–S76.

Magistrale, H., K. McLaughlin, and S. Day (1996). A geology based 3-D velocity model of the Los Angeles basin sediments. *Bulletin of the Seismological Society of America 86*, 1161–1166.

Osteraas, J. D. and H. Krawinkler (1990). Strength and ductility considerations in seismic design. Technical Report BLUME-90, 1990-08, The John A. Blume Earthquake Engineering Center, Stanford, California.

SAC (1995). Analytical and field investigations of buildings affected by the Northridge earthquake of January 17, 1994 – Part 2. Technical Report SAC 95-04, Part 2, Structural Engineers Association of California, Applied Technology Council, and California Universities for Research in Earthquake Engineering, USA.

Stewart, J. P., R. B. Seed, and G. L. Fenves (1998). Empirical evaluation of inertial soil-structure interaction effects. Technical Report PEER-98/07, Pacific Earthquake Engineering Center, University of California, Berkeley, California, USA.

Suss, M. P. and J. H. Shaw (2003). P-wave seismic velocity structure derived from sonic logs and industry reflection data in the Los Angeles basin. *Journal of Geophysical Research 108*(B3), Article no. 2170.

Trifunac, M., M. Todorovska, and T. Hao (2001). Full-scale experimental studies of soil-structure interaction – a review. In *Proceedings of the Second US–Japan Workshop on Soil-Structure Interaction, Tsukuba City, Japan, 52 pages (published on CD-ROM)*.

Wald, D. J., T. H. Heaton, and K. W. Hudnut (1996). A dislocation model of the 1994 Northridge, California, earthquake determined from strong-motion, GPS, and leveling-line data. *Bulletin of the Seismological Society of America 86*, S49–S70.